JOURNAL OF SOLID STATE CHEMISTRY 55, 270–279 (1984)

On the Topotactic Dehydration of $VOHPO_4 \cdot 0.5\ H_2O$ into Vanadyl Pyrophosphate

E. BORDES* AND P. COURTINE

Département de Génie Chimique, Université de Technologie de Compiègne, B.P. 233, 60206 Compiègne Cedex, France

AND J. W. JOHNSON

Exxon Research and Engineering Company, Route 22 East, Annandale, New Jersey 08801

Received January 23, 1984; in revised form June 13, 1984

The thermal analysis (DTA, TGA) of the dehydration under inert atmosphere of the vanadyl hydrogen phosphate hydrate $VOHPO_4 \cdot 0.5\ H_2O$ recently studied, together with the characterization of both starting and final compounds (XRD, ir, and uv–visible spectroscopies) show that pseudomorphic vanadyl pyrophosphate is obtained in these conditions. This form γ-$(VO)_2P_2O_7$ is the active and selective catalyst in butane oxidation to maleic anhydride whereas β-$(VO)_2P_2O_7$ is selective in butene oxidation only. Pseudomorphic relations between $VOHPO_4 \cdot 0.5\ H_2O$ and γ-$(VO)_2P_2O_7$ are evidenced by the comparison of XRD patterns, SEM and TEM experiments, and justified with the help of both structures. The low values of the activation energies calculated from kinetic data, $E_1 = 21.4$ and $E_2 = 24.7$ kcal $\cdot$ mole^{-1} show that the dehydration of the hydrate and the formation of γ are topotactic, this hypothesis is confirmed and the mechanism stated precisely in view of the preceding results.

Introduction

Vanadyl pyrophosphate $(VO)_2P_2O_7$ is an active and selective catalyst for the mild oxidation of butenes (*1–3*) or butane (*4–6*) to maleic anhydride. The redox system 2 $VOPO_4/(VO)_2P_2O_7$ is involved in these reactions according to the Mars and Van Krevelen mechanism (*1, 7*). This kind of heterogeneous catalysis belongs to the so-called "structure sensitive reactions" (*8–13*), because the different morphologies of the bulk of the crystalline catalyst can be related to the different values of the selectivity in maleic anhydride (*17*). In turn, the morphology of the crystallites is related to the method of preparation which determines the nature of the precursor delivering the catalytic phase after activation.

The aim of this paper is to study one of the methods of preparation leading to a particular morphology of $(VO)_2P_2O_7$, to which we shall refer as "γ-$(VO)_2P_2O_7$"; the thermal decomposition in an inert atmosphere of the new precursor $VOHPO_4 \cdot 0.5\ H_2O$ recently characterized (*13*) yields samples of γ-$(VO)_2P_2O_7$ having a strongly lamellar

* To whom any correspondence should be addressed.

0022-4596/84 $3.00

structure. The pseudomorphic relations between the starting and the final products obtained by a topotactic reaction will be discussed in terms of their structural and kinetic properties.

Experimental

1. Preparation

Vanadium(V) phosphate dihydrate $VOPO_4 \cdot 2\ H_2O$ (*14, 15*) was refluxed with stirring in 2-butanol for 20 hr. After cooling, the resulting solid was filtered and washed several times with acetone. The resulting light-blue solid was dried *in vacuo* for 8 hr and identified as $VOHPO_4 \cdot 0.5\ H_2O$ (*16*) by XRD, ir spectroscopy, and chemical analysis.

2. Thermal Decomposition

2.1. Preparation of γ-$(VO)_2P_2O_7$. $VOHPO_4 \cdot 0.5\ H_2O$ was placed in an alumina or platinum boat inside a silica tube placed in an electric furnace. Nitrogen was passed through the tube while heating and the partial pressure of oxygen measured on an oxygen analyzer ($pO_2 \cong 5 \times 10^{-5}$ atm). The temperature was raised to 750°C (100°C · hr^{-1}) and maintained at this value for 3 hr. The resulting grey solid was analyzed as γ-$(VO)_2P_2O_7$ by the same methods as above.

2.2. Thermal analysis. TGA and DTA were performed, respectively, in Setaram microbalance and semimicroanalyzer at various heating rates under N_2 flow. For the kinetic study, the sample was introduced in the microbalance already heated at the desired temperature (300–410°C) and the loss of weight recorded in isothermal conditions with constant N_2 flow (3 liters · hr^{-1}); when the weight was constant, the temperature was raised to 750°C to recover the stoichiometry in oxygen of $(VO)_2P_2O_7$.

2.3. Structural analysis. XRD patterns were obtained on CGR Guinier camera (X-ray transmission, Cu$K\alpha$ radiation) and on diffractometer (X-ray reflection, Co$K\alpha$); in this last case, the powdered sample was pressed by hand on the sample holder.

Scanning (SEM) and transmission (TEM) electron microscopies were performed respectively, on Cameca and Jeol 100 C at 100 kV.

Infrared spectra (4000–250 cm^{-1}) were carried on a Perkin–Elmer 451 spectrometer, using KBr disk technique. Ultraviolet–visible diffuse reflectance spectra of powdered samples were obtained on a Beckmann DK2A spectrophotometer from 5000 to 50,000 cm^{-1}, with or without dilution with MgO.

Results

1. Thermal Decomposition of $VOHPO_4 \cdot 0.5\ H_2O$

According to DTA at heating rates between 300 and 1200°C · hr^{-1}, the water molecules are lost in two steps near 365 and 460°C (Fig. 1); very small exothermic peaks are seen at $500 < t < 800$°C, the first one at 560°C being observed whatever the heating rate.

The shape of the thermogravimetric curves in TGA depends strongly on the

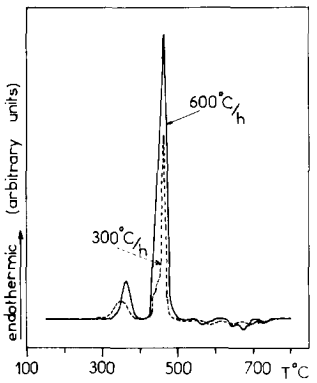

FIG. 1. DTA of $VOHPO_4 \cdot 0.5\ H_2O$ dehydration (N_2 flow 1 liter · hr^{-1}). Heating rates: solid line 600°C · hr^{-1}; dashed line 300°C · hr^{-1}.

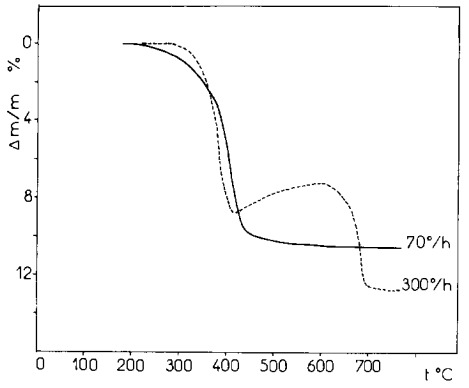

FIG. 2. Thermogravimetric curves of $VOHPO_4 \cdot 0.5\ H_2O$ dehydration (N_2 flow). Heating rates: solid line 70°C · hr^{-1}; dashed line, 300°C · hr^{-1}.

TABLE I

RATE CONSTANTS FOR THE TWO STEPS OF $VOHPO_4 \cdot 0.5\ H_2O$ DEHYDRATION

T (°K)	$k_1 \times 10^{-2}$ (min^{-1})	$k_2 \times 10^{-2}$ (min^{-1})
568	0.617	0.717
585	0.497	0.923
599	1.110	2.134
609	1.333	2.000
610	2.067	3.186
628	1.911	3.596
638	2.286	6.512
648	3.333	6.993
680	6.454	9.366

heating rate (Fig. 2) and adsorbed water can be mistaken for crystal water if the heating rate is too high. At 70°C · hr^{-1} the unique and continuous loss of weight from 300 to 450°C corresponds approximately to the theoretical percentage (10.46%). At higher rates (140–700°C · hr^{-1}), the loss of water is superimposed near 420°C to a partial reoxidation which stops near 630°C; the consecutive reduction and final loss occur between 630 and 750°C, which amounts to 11.6% (Fig. 2). When isothermal experiments are performed at temperatures lower than 420°C the total weight loss is 8.3%, and two steps, each of 1%, occur near 510 and 700°C; if the experiment is stopped at 700°C (9.3%) a green–brown product is found, the XRD pattern of which is identical to a poorly crystallized $(VO)_2P_2O_7$ sample (*1, 7*) except the (020) line which is very weak instead of strong. If the experiment is continued to 730°C (10.3%), the powder is greenish-gray and its pattern identical to $(VO)_2P_2O_7$ pattern.

In the kinetic experiments carried out in isothermal conditions, in a sufficiently large range (100°C), no partial oxidation occurs. The sigmoidal shape of the thermogravimetric isotherms, with a relatively long period of induction, suggests that this endothermic decomposition is autoaccelerated (Table I, Fig. 3). On each side of the bending point the isotherms obey formally the Prout and Tompkins law (*18*):

$$\log \frac{x}{1-x} = k_1 t + C \qquad 0.25 < x < 0.50 \quad (1)$$

$$\log \frac{x}{1-x} = k_2 t + C' \qquad 0.50 < x < 0.95 \quad (2)$$

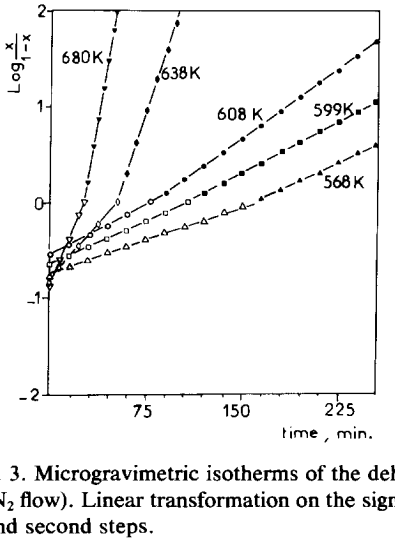

FIG. 3. Microgravimetric isotherms of the dehydration (N_2 flow). Linear transformation on the sigmoids, first and second steps.

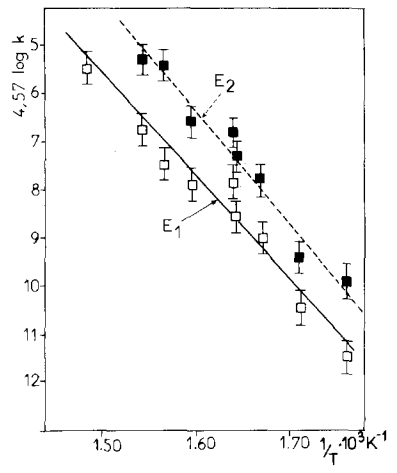

FIG. 4. Arrhenius plots in the temperature range 307–407°C.

in which x is the degree of conversion. Other laws established by Avrami and Erofeev (*18*) such as

$$\log(1 - x) = -kt^n \qquad (3)$$

have been tried also but they do not fit exactly the isotherms.

Arrhenius plots in the temperature range 307–407°C are presented in Fig. 4. The activation energies calculated before and after the bending point by the least-square method amount to $E_1 = 21.4$ and $E_2 = 24.7$ kcal · mole^{-1}, respectively.

2. *Structural Features of* γ-$(VO)_2P_2O_7$

2.1. Infrared and uv–visible spectra. The ir spectra of γ-$(VO)_2P_2O_7$ are better resolved than those of the $(VO)_2P_2O_7$ samples already studied (*1, 7*); the main bands are situated at the same wavenumbers but sharper (Fig. 5). In uv–visible spectroscopy, the vanadyl ion (VO^{2+}) is known to present two or three bands due to *d–d* transitions in the crystal field range (*19*); however, the number and the wavenumbers of these bands are not exactly the same for all the samples of $(VO)_2P_2O_7$ according to the origin and the color of the product (Table II), which account for small variations of symmetry in the oxygen environment of the vanadium atom.

2.2. XRD patterns. The Seeman–Bohlin patterns of both γ and usual $(VO)_2P_2O_7$ are similar, but on the contrary the diffractograms show that the relative intensities I/I_0 of the main lines are changed according to the nature of the precursor (Table III). This has already been observed for α-$(VO)_2P_2O_7$ obtained by a fast reduction of α-$VOPO_4$ (*7*). The use of the X-ray reflexion method allows indeed to evidence the effect of orientation of platelets on the sample holder: the more layered is the structure, the more intense are the lines which correspond to the concerned cleavage planes (*20*). Small differences in the intensity of some lines are also detected: in TGA experiments stopped at 700°C, the intensity of (020) γ-$(VO)_2P_2O_7$ is weak instead of strong.

2.3. SEM and TEM experiments. SEM micrographs show that the dehydration of $VOHPO_4 \cdot 0.5\ H_2O$ occurs without altering the gross morphology of the crystallites (Fig. 6). TEM experiments confirm this fact at the lower scale: the platelet crystals of the hydrate have well-defined outlines and present always the same plane indexed as (010) (Fig. 7). When the crystal is thin, bubbles occur under the action of the beam and the diffraction pattern vanishes.

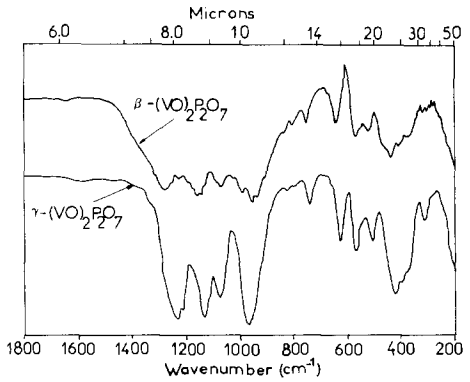

FIG. 5. Infrared spectra of γ-$(VO)_2P_2O_7$ and of β-$(VO)_2P_2O_7$ (1800–200 cm^{-1}).

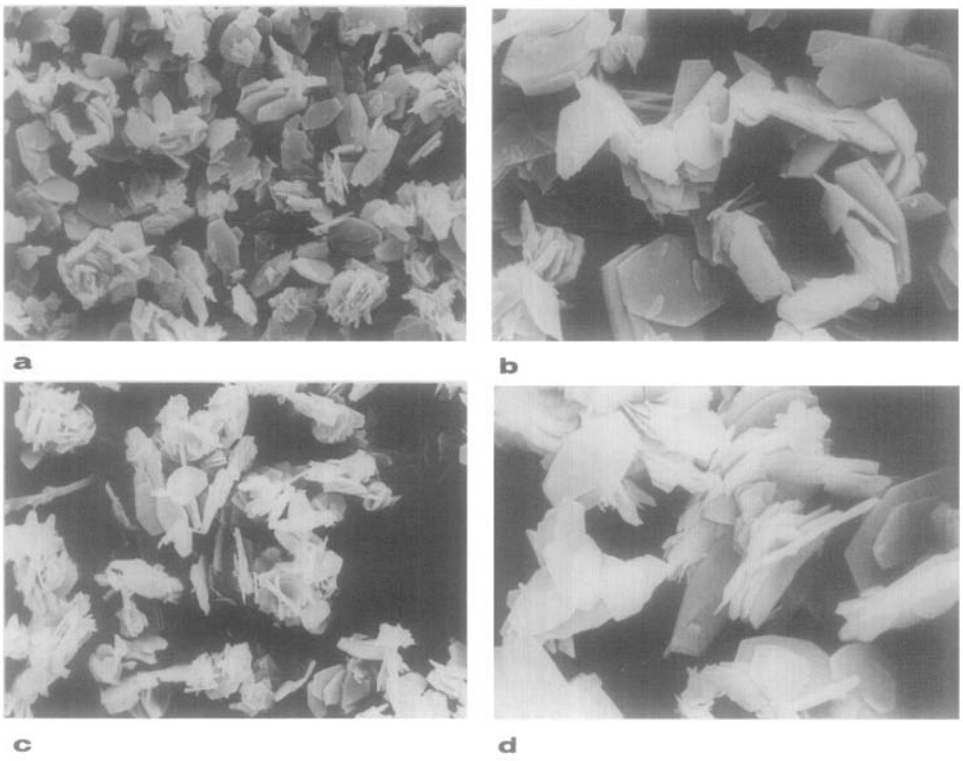

FIG. 6. SEM: $VOHPO_4 \cdot 0.5\ H_2O$, (a) 2000×; (b) 6000×; after dehydration (500°C): (c) 2000×; (d) 6000×.

TABLE II

ULTRAVIOLET–VISIBLE DIFFUSE REFLECTANCE SPECTRA

Vanadyl compounds	Crystal field bands, $\bar{\nu}$ (cm^{-1})			Charge transfer bands $\bar{\nu}$ (cm^{-1})	
	$2_{B_2} \rightarrow 2_E$	$2_{B_2} \rightarrow 2_{B_1}$	$2_{B_2} \rightarrow 2_{A_1}$		
$VOHPO_4 \cdot 0.5\ H_2O$	12,100	14,900	22,200 (sh)	27,800 (sh)	40,000
γ-$(VO)_2P_2O_7$[a]	11,350	15,300	20,800 (sh)	—	35,100
γ-$(VO)_2P_2O_7$[b]	11,350 12,050 (sh)	15,300	—	—	35,100
β-$(VO)_2P_2O_7$[c]	11,750 13,400 (sh)	15,600	21,300 (sh)	—	33,330

[a] Sample obtained by dehydration of $VOHPO_4 \cdot 0.5\ H_2O$ at 730°C.
[b] Sample obtained at 700°C.
[c] Sample obtained by reduction of β-$VOPO_4$ at 760°C (*1*, *7*), (sh): shoulder.

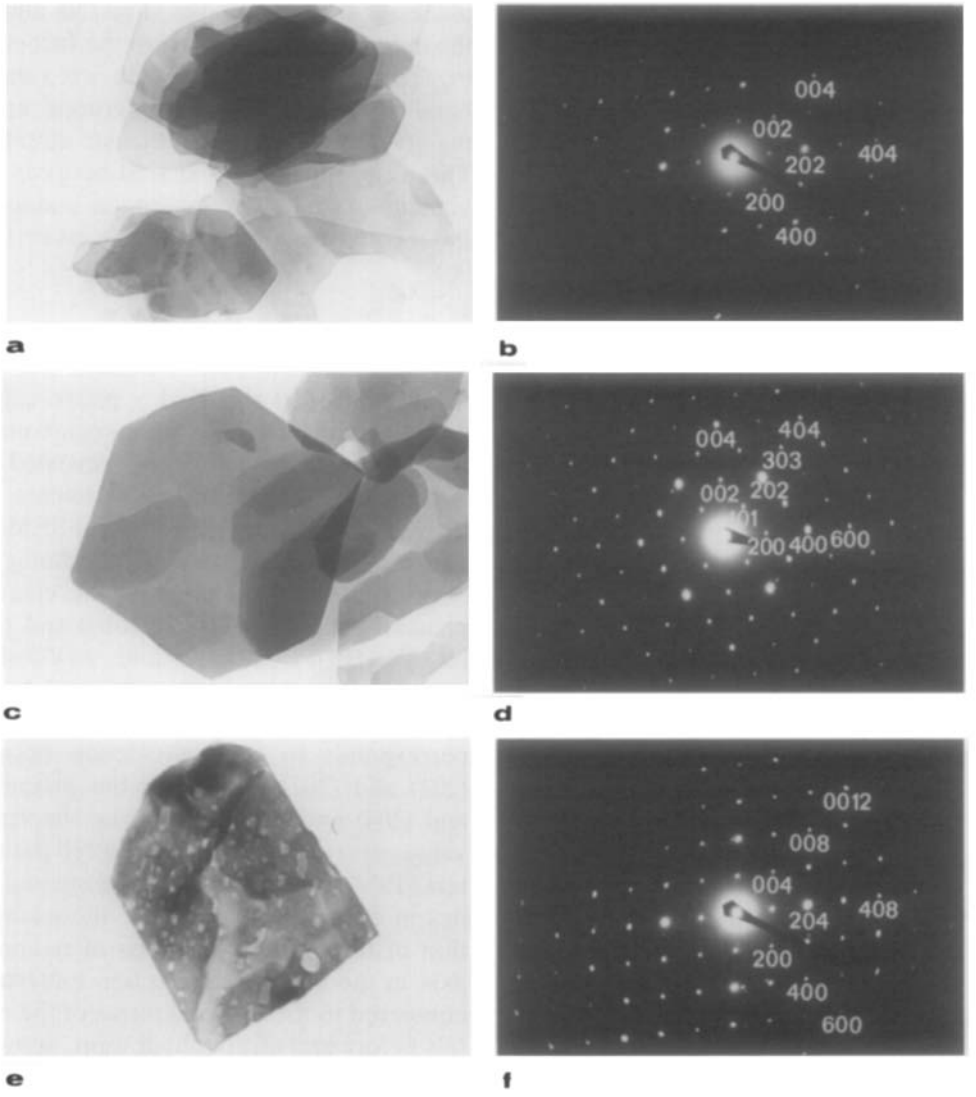

FIG. 7. TEM: $VOHPO_4 \cdot 0.5\ H_2O$, (a) platelets, 33,000×; (b) diffraction (010) plane; (c) crystal, 50,000×; and (d) diffraction (010); γ-$(VO)_2P_2O_7$ (obtained at 750°C); (e) crystals, 100,000×; and (f) diffraction (020) plane.

The samples of γ-$(VO)_2P_2O_7$ have the same lamellar morphology as the precursor and the electron diffraction patterns display always the plane (020) of $(VO)_2P_2O_7$; sometimes, small growing microcrystals are seen to be oriented on a larger crystal (Fig. 7). On the contrary when samples of $(VO)_2P_2O_7$ prepared by reduction of β-$VOPO_4$ were examined in TEM, various planes such as (100), (011), (110), and never (020), were observed by diffraction (*7*).

Discussion

1. Structural Relations between $VOHPO_4 \cdot 0.5\ H_2O$ and γ-$(VO)_2P_2O_7$

The structure of $(VO)_2P_2O_7$ has been solved separately by two groups of workers

TABLE III

COMPARISON BETWEEN THE INTENSITIES OF (*hkl*) LINES OF $VOHPO_4 \cdot 0.5\ H_2O$ AND (*h'k'l'*) LINES OF $(VO)_2P_2O_7$ SAMPLES OF DIFFERENT ORIGIN

$VOHPO_4 \cdot 0.5\ H_2O$			$(VO)_2P_2O_7$			
			γ		β	α
d (Å)	*hkl*	I/I_0	I/I_0	*h'k'l'*	I/I_0	I/I_0
5.90	101	3	3	102	9	—
5.719	010	100	100	020	89	100
4.818	200	2	4	200	13	—
4.099	111	5	—	111	14	—
2.944	202	35	75	204	100	4
	301		41	302	60	3
2.047	222	6	12	224	23	—
1.960	303	2	10	306	35	—
			5	040	12	10
$a = 9.620$ Å $b = 5.699$ Å $c = 7.434$ Å $Pmn2_1$		(*16*)	$a' = 9.571$ Å $b' = 7.728$ Å $c' = 16.568$ Å $Pbc2_1{}^a - C_{2v}^5$			(*21*)

[a] $Pbc2_1$ is an unconventional setting chosen to get vanadyl bonds parallel to *b* axis (*21*).

(*21, 22*) who gave the same space group C_{2v}^5 and found close values of the cell parameters. However the resolution factor was not the same ($R_w \sim 0.18$ and $R \sim 0.09$ for Refs. (*21, 22*), respectively), and in the second case no indication of the method of preparation was given. In a parallel plane to (010) (*21*), the framework is composed with pairs of pseudooctahedra sharing an edge (the vanadyl bonds being in a *trans*-position) linked by phosphate tetrahedra (Fig. 8); the layers are held together by asymmetrical V=O · · · V bonds and P—O—P (bent) bonds of P_2O_7 in the direction *b*. The two groups of authors are in disagreement about the relative succession of the tetrahedra along *c* which depends also on the different values of P—O—P angles they find.

The single-crystal structure of the acid hydrate $VOHPO_4 \cdot 0.5\ H_2O$ has just been solved (*16*), which allows to establish the structural analogies between the (010) planes of the two phases (Figs. 9a and b): the main differences concern the face-sharing pairs of octahedra with *cis*-vanadyl bonds in *ac* planes and HPO_4 groups replacing $\frac{1}{2}(P_2O_7)$ in the perpendicular direction. The water molecule is shared between two vanadium atoms and hydrogen bonded to P–OH groups in the adjacent layer (Fig. 9b).

2. *Pseudomorphic Relations*

The pseudomorphic relations between the hydrate and the final γ phase can be firmly established from the comparison between their morphologies revealed by XRD, TEM, and SEM experiments and their crystal structures. TEM and SEM evidence the strongly lamellar morphology of both crystalline compounds, the cleavage planes being, respectively (010) and (020) for $VOHPO_4 \cdot 0.5\ H_2O$ and γ-$(VO)_2P_2O_7$ (Fig. 10). The value of the angle α is close to 104° as measured on micrographs, which corresponds to the intersection between $(20\bar{2})$ and (202) planes for the precursor, and $(20\bar{4})$ and (204) for γ. The theoretical values of α calculated from the cell parameters (Table III) fit well the experimental values in each case. Moreover, the examination of the relative positions of reciprocal axis in the electron diffraction patterns as compared to the external forms of the crystals before and after dehydration, allows to

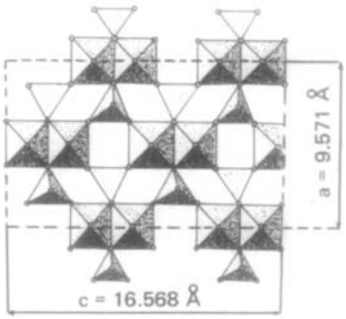

FIG. 8. Crystal structure of $(VO)_2P_2O_7$ according to the (*21*): (010) plane.

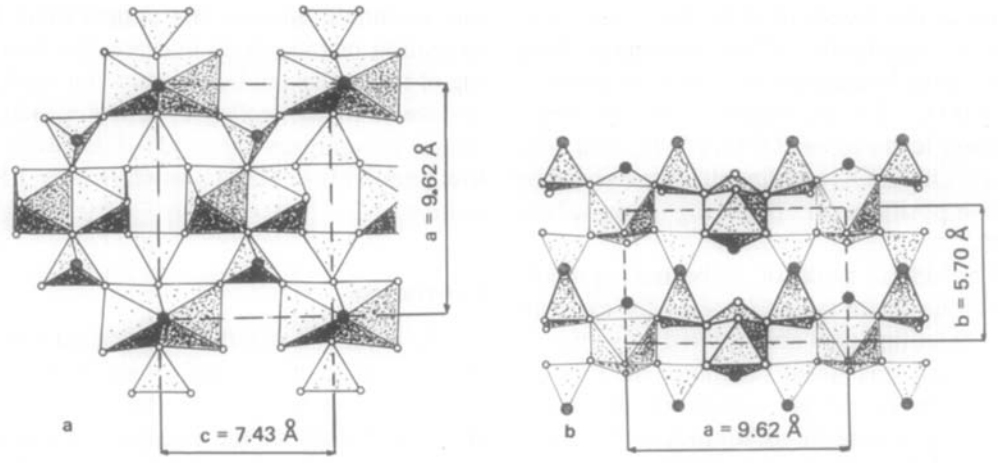

FIG. 9. Crystal structure of $VOHPO_4 \cdot 0.5\ H_2O$ (*16*): (a) (010); (b) (001); white circles, O; dashed circles, O(H); full circles, $O(H_2)$.

conclude that, during the reaction, the orientations of x, z as compared to y, are kept parallel to x', z', as compared to y'.

At last, the pseudomorphism is confirmed by XRD (by reflection) from which the relation observed between the relative intensities I/I_0 of $(0k0)$, $(0k'0)$ lines on one hand, $(h0l)$, $(h'0l')$ on the other (Table III) is in accordance with the idea that the (010) plane of the precursor is topologically equivalent to the (020) plane of γ-$(VO)_2P_2O_7$; the values for $a = 9.62$ and $a' = 9.57$ Å, and $c = 7.43$, not very far from $c'/2 \sim 8.3$ Å, are close to each other.

3. *Topotactic Mechanism of Dehydration*

From DTA and TGA experiments, it is seen that $VOHPO_4 \cdot 0.5\ H_2O$ retains its water of hydration tenaciously up to 350°C and that the occurrence of a partial reoxidation is very sensitive to the heating rate. The small successive losses of weight, already observed in the high-temperature decomposition of $VOHPO_4 \cdot 0.5\ H_2O$ (*15*), corresponding to the small DTA peaks above 500°C, give evidence about the instability of the solid. These phenomena could be attributed to a kind of stacking disorder, before the final reorganization of the layers yielding γ-$(VO)_2P_2O_7$: they are related also to the weak differences observed in uv spectroscopy (Table II) and XRD patterns (Table III), concerning, respectively, the symmetry of the (VO_6) pseudooctahedra and the periodicity of the lattice perpendicularly to the ac plane of $(VO)_2P_2O_7$.

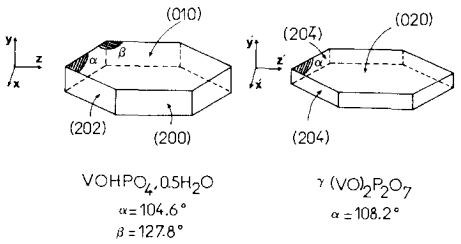

FIG. 10. Pseudomorphic relations between the crystals of $VOHPO_4 \cdot 0.5\ H_2O$ and γ-$(VO)_2P_2O_7$.

The sigmoidal shape of the thermogravimetric isotherms corresponding to an autoaccelerated reaction, and the weak values of the activation energies E_1 and E_2 show that the water molecules are cooperatively expelled from the lattice of the hydrate constituted by sheets $(VOHPO_4)_\infty$. Such a cooperative dehydration means that these groups are located between the sheets constituted by the framework $(VOHPO_4)_\infty$. In addition, these sheets being structurally re-

lated to the layers of $(VO)_2P_2O_7$, the reaction is topotactic. Other examples have been already encountered with the cases of $VOHPO_4 \cdot 2\ H_2O$, which reversible dehydration leads to α-$VOPO_4$ (*7, 15*) and with $NH_4VOOHPO_4$, yielding the same phase by decomposition in oxidizing atmosphere (*23*).

The kinetic model of the branching mechanism has been studied mainly for exothermic reactions (*18*) and applied to some endothermic gas–solid reactions such as the reduction of cobalt sulfate by hydrogen (*24*). According to such models, the topotactic dehydration of $VOHPO_4 \cdot 0.5\ H_2O$ would begin by the deformation of the sheets inducing cracks allowing the evacuation of more and more H_2O molecules and the chain propagation of the reaction in the solid.

The first endothermic step concerns the shared water molecules, the loss of which results in vacancy formation at the apex of the octahedra; very probably at this stage an electronic rearrangement proceeds, and *cis*-vanadyl reorganize into *trans*-vanadyl bonds, which corresponds to the formation of layers $(VOHPO_4)_\infty$ very close to the framework (010) of $(VO)_2P_2O_7$ (Figs. 8 and 9). The rate-limiting step of the first part of the reaction (E_1 = 21.4 kcal · mole^{-1}) would be therefore the gradual cooperative deformation of the framework due to the escape of 0.5 H_2O by mole.

The second part of the reaction (E_2 = 24.7 kcal · mole^{-1}) concerns the progressive joining of the sheets: to replenish the vacancies, the layers tend to join themselves which helps to expell other water molecules obtained this time from two (HPO_4) groups, followed by crystallization of γ-$(VO)_2P_2O_7$. The different intensities of the two main DTA peaks as well as the values of activation energies account for the two different kinds of H_2O expelled. On the other hand, the unique and continuous loss of weight in TGA means that the starting of one molecule induces the cooperative dehydration of the whole hydrate: the breaking of the hydrogen bonds between the layers leads to the collapse of the structure which reorganizes into $(VO)_2P_2O_7$ even at low temperature (420°C) as shown by XRD patterns.

Conclusion

The present work throws light on one of the criteria governing the selectivity in mild oxidation catalysis, e.g., the influence of the morphology of the catalyst, which can be controlled by the preparation and the nature of the precursor. The previous characterization of $VOHPO_4 \cdot 0.5\ H_2O$ (*16*), precursor of the selective catalyst in butane oxidation, and misidentified as $(VO)_2P_2O_7 \cdot 2\ H_2O$ by other authors (*25*), is here confirmed by our experiments. The pseudomorphic relations between the hydrate and γ-$(VO)_2P_2O_7$ shown by XRD, SEM, TEM are established in view of the two structures which allows also to explain the topotactic mechanism of dehydration.

Slight structural differences exist between the γ form and the already characterized β-$(VO)_2P_2O_7$ sample obtained by reduction of β-$VOPO_4$ (*1, 15*). Up to now, it is not ascertained whether "β" and "γ" forms are real different polymorphs of $(VO)_2P_2O_7$ (with different space groups) or if they are only pseudomorphs, and we are still studying this problem. However, the striking difference is observed for the reactivity of each form, according to their chemical properties. First, γ-$(VO)_2P_2O_7$ is obtained by a topotactic decomposition of a V(IV) compound, while α or β-$VOPO_4$ yield β-$(VO)_2P_2O_7$ by reduction near 750°C in the same atmosphere (N_2, $pO_2 \sim 5 \times 10^{-5}$ atm). Second, the reoxidation of γ-$(VO)_2P_2O_7$ under pO_2 = 1 atm yields two new polymorphs, δ and γ-$VOPO_4$ (*26*), according to the temperature, while β-$(VO)_2P_2O_7$ is reoxidized in the β-$VOPO_4$

form only. The study of the structural and thermodynamic properties of δ and γ-$VOPO_4$ is in progress in order to compare the new redox γ-$VOPO_4$/γ-$(VO)_2P_2O_7$, active and selective in butane oxidation, to the redox β-$VOPO_4$/β-$(VO)_2P_2O_7$ active and selective in butene oxidation to maleic anhydride. Recent information (*27*) demonstrates that γ-$(VO)_2P_2O_7$ exhibits high selectivity and activity in the oxidation of butane to maleic anhydride.

References

1. E. Bordes, and P. Courtine, *J. Catal.* **57,** 236 (1979).
2. L. Morselli, A. Riva, F. Trifiro, M. Zucchi, and G. Emig, *Chim. Ind. (Milan)* **10,** 791 (1978).
3. H. Seeboth, G. Ladwig, B. Kubias, H. Wolf, and B. Lucke, *Ukr. Khim. Zh.* **8,** 842 (1977).
4. H. Wolf, N. Wustneck, M. Seeboth, V. M. Belousov, and V. A. Zazigalov, *Z. Chem.* **22,** 193 (1982).
5. M. Brutovsky and S. Gerej, *Collect. Czech. Chem. Commun.* **47,** 403 (1982).
6. G. Martini, L. Morselli, A. Riva, and F. Trifiro, *React. Kinet. Catal. Lett.* **8,** 431 (1978).
7. E. Bordes, thesis, Compiègne, France (1979).
8. M. Boudart, "Advances in Catalysis," Vol. 26, p. 153, Academic Press, New York (1969).
9. A. Vejux and P. Courtine, *J. Solid State Chem.* **23,** 93 (1978).
10. M. Inomata, A. Miyamoto, and Y. Murakami, *J. Phys. Chem.* **85,** 2372 (1981).
11. J. C. Volta, M. Forissier, F. Theobald, and T. P. Pham, "Selectivity in Heterogeneous Catalysis," Faraday Discuss. 72/13, Nottingham, Alameda (1981).
12. J. M. Tambouet and J. E. Germain, *J. Catal.* **72,** 375 (1981).
13. J. Ziółkowski, *J. Catal.* **80,** 263 (1983).
14. G. Ladwig, *Z. Anorg. Allg. Chem.* **338,** 266 (1965).
15. E. Bordes, P. Courtine, and G. Pannetier, *Ann. Chim.* **8,** 105 (1973).
16. J. W. Johnson, D. C. Johnston, A. J. Jacobson, and J. F. Brody, submitted for publication; M. E. Leonowicz, J. W. Johnson, A. J. Jacobson, *J. Amer. Chem. Soc.*, in press.
17. E. Bordes, P. Courtine, and J. W. Johnson, in preparation.
18. W. E. Garner, "The Chemistry of the Solid State," Butterworth, London (1956).
19. R. J. H. Clarke, "The Chemistry of Titanium and Vanadium," Elsevier, Amsterdam (1968).
20. A. Guinier, "Théorie et technique de la radiocristallographie," Dunod, Paris (1970).
21. N. Middlemiss, thesis, McMaster University, Hamilton, Canada (1978).
22. Yu. Gorbunova and S. A. Linde, *Dokl. Akad. Nauk SSSR* **245,** 584 (1979).
23. S. Pulvin, E. Bordes, M. Ronis, and P. Courtine, *J. Chem. Res.* **S 29,** M 362 (1981).
24. P. Courtine, *Bull. Soc. Chim. Fr.* 2850 (1963).
25. G. Poli, I. Resta, O. Ruggeri, and F. Trifiro, *Appl. Catal.* **1,** 395 (1981).
26. E. Bordes, P. Courtine, and J. W. Johnson, "10th International Symposium on the Reactivity of Solids, Dijon, France" (1984).
27. T. C. Yang, K. K. Rao, and I. Huang, U.S. Patent No. 4,392,986 (1983).